Which Is the More Effective Driver of the Poleward Eddy Heat Flux Variability: Zonal Gradient of Tropical Convective Heating or Equator-to-Pole Temperature Gradient?

MINGYU PARK^a AND SUKYOUNG LEE^a

^a Department of Meteorology and Atmospheric Science, The Pennsylvania State University, University Park, Pennsylvania

(Manuscript received 5 October 2021, in final form 16 January 2022)

ABSTRACT: Future projections of the poleward eddy heat flux by the atmosphere are often regarded as being uncertain because of the competing effect between surface and upper-tropospheric meridional temperature gradients. Previous idealized modeling studies showed that eddy heat flux response is more sensitive to the variability of lower-tropospheric temperature gradient. However, observational evidence is lacking. In this study, observational data analyses are performed to examine the relationships between eddy heat fluxes and temperature gradients during boreal winter by constructing daily indices. On the intraseasonal time scale, the surface temperature gradient is found to be more effective at regulating the synoptic-scale eddy heat flux (SF) than is the upper-tropospheric temperature gradient. Enhancements in surface temperature gradient, however, are subject to an inactive planetary-scale eddy heat flux (PF). The PF in turn is dependent on the *zonal* gradient in tropical convective heating. Consistent with these interactions, over the past 40 winters, the zonal gradient in tropical heating and PF have been trending upward, while the surface temperature gradient and SF have been trending downward. These results indicate that for a better understanding of eddy heat fluxes, attention should be given to zonal convective heating gradients in the tropics as much as to meridional temperature gradients.

KEYWORDS: Planetary waves; Diabatic heating; Synoptic-scale processes; Upper troposphere; Heat budgets/fluxes; Surface temperature

1. Introduction

The projected tropospheric temperature response under global warming scenarios is often characterized by a "tug-of-war" between increased meridional temperature gradient in the upper troposphere that owes to enhanced tropical upper-tropospheric warming, and decreased meridional temperature gradient at the near-surface caused by Arctic amplification (O'Gorman 2010; Barnes and Polvani 2015; Vallis et al. 2015). Because the atmospheric circulation responses to these opposite changes in the equator-to-pole temperature gradients may compensate each other (Butler et al. 2010; Shaw et al. 2016; Screen et al. 2018), this tug-of-war has been regarded as a source of uncertainty in the projected climate change (Cattiaux and Cassou 2013; Harvey et al. 2014; Barnes and Polvani 2015).

The premise of the tug-of-war is that the climate response in question—e.g., storm tracks, jets—is realized through baroclinic eddies which respond to meridional temperature gradients. Prior studies have attempted to address this question by investigating the eddy response to changes in the meridional temperature gradients using numerical models (Held and O'Brien 1992; Pavan 1996; Lunkeit et al. 1998; Yuval and Kaspi 2016, 2020). By employing a three-layer quasigeostrophic (QG) model, Held and O'Brien (1992) examined the sensitivity of eddy fluxes to upper- and lower-level vertical wind shear (which is equivalent to the meridional temperature gradient in that layer)

© Supplemental information related to this paper is available at the Journals Online website: https://doi.org/10.1175/JAS-D-21-0262.s1.

Corresponding author: Mingyu Park, mup65@psu.edu

and found that eddy fluxes in their model are more sensitive to changes in lower-level vertical shear (their Fig. 8). A consistent conclusion was drawn by Pavan (1996) and Lunkeit et al. (1998), who, respectively, used a multilayer QG model and a simplified global circulation model (GCM). More recently, Yuval and Kaspi (2016, 2020) attempted to address this question using the dry dynamical core of a GCM. When the model temperature profile is forced to mimic the temperature trends in a global warming scenario, their results showed that the eddy heat flux response is more sensitive to the lower-level temperature gradient (Yuval and Kaspi 2020, their Figs. 6 and 7).

In this study, we examine the sensitivity of the eddy heat fluxes to changes in the mean temperature gradient using an observational dataset. Because baroclinic eddy time scale is on the order of days, complementing these modeling studies, daily observational data can be used instead to examine whether and to what extent eddy heat fluxes respond to the meridional temperature gradients on the intraseasonal time scale. In addition, Chemke and Polvani (2020) showed that over the most recent four decades, across reanalysis products, there have been declining trends of the Northern Hemisphere annual-mean eddy heat fluxes in the lower troposphere. This eddy heat flux trend is correlated with the decreasing trend of the surface meridional temperature gradient which primarily reflects the Arctic warming. Motivated by this recent finding, we also examine the interdecadal variability of the upper tropospheric and the surface temperature gradient and its linkage to the eddy heat flux variability.

Another source of eddies that participate in the observed poleward heat transport is the zonally varying tropical convective activities. Examining the life cycles of planetary-scale (zonal wavenumbers k = 1–3) and synoptic-scale waves (zonal wavenumbers k = 4–72) separately, Baggett and Lee (2015) showed that planetary-scale eddies excited by localized tropical convection effectively tap zonal available potential energy and enhance poleward heat transport. In fact, the planetary-scale eddy contribution to poleward heat transports and subsequent Arctic surface temperature change is dominant over the contribution by synoptic-scale eddies (Baggett and Lee 2015; Graversen and Burtu 2016). Other recent studies supported this finding by showing that Arctic temperature variability is affected by poleward-propagating planetary-scale eddies excited from the localized tropical diabatic heating (Lee et al. 2011; Yoo et al. 2012; Goss et al. 2016; Park and Lee 2019, 2021). Therefore, we also investigate the relationship between eddy heat flux and an index that measures the degree of zonal asymmetry in tropical convective heating. The result will then be compared with the relationships between eddy heat flux and the equator-to-pole temperature gradients. Although orography also plays a role in driving planetary-scale circulation (e.g., Held et al. 2002), it is not considered in this study.

2. Data and method

In this study, we use temperature and meridional wind from the fifth generation of the European Centre for Medium-Range Weather Forecasts (ECMWF) reanalysis (ERA5; Hersbach et al. 2020) for the period spanning from 1979/80 to 2018/19 December to February (DJF). The daily mean data are used by averaging four 6-hourly fields with a $1.25^{\circ} \times 1.25^{\circ}$ horizontal resolution and 37 pressure levels. Potential vorticity data are used to indicate the dynamic tropopause by the 2 potential vorticity unit (PVU; 10^{-6} K kg $^{-1}$ m $^{-2}$ s $^{-1}$) isoline.

Throughout the study, eddy is defined as a deviation from the zonal mean, and eddy heat flux is denoted by $|v^*\theta^*|$, where v indicates meridional wind and θ indicates potential temperature. The brackets indicate the zonal mean and the asterisk indicates a deviation therefrom. Although it is well established that transient, synoptic-scale eddy heat fluxes follow the flux-gradient relationship (e.g., Green 1970; Lorenz 1979; Kushner and Held 1998; Franchito and Rao 2003), motivated by a recent finding that planetary-scale eddy growth is independent of the meridional temperature gradient and zonal available potential energy (Baggett and Lee 2015), we separate eddy heat fluxes into planetary-scale (zonal wavenumbers 1-3; hereafter, PF) and synopticscale (zonal wavenumbers greater than or equal to 4; SF) contributions, and denote them by $|v_p^*\theta_p^*|$ and $|v_s^*\theta_s^*|$, respectively. The results are qualitatively unchanged if zonal wavenumber 3 is excluded from the PF and if zonal wavenumbers larger than 10 are excluded from SF. A daily mean eddy heat flux is obtained by averaging the four 6-hourly fluxes, and its daily anomaly is obtained by removing a seasonal cycle that retains the first 10 harmonics of the calendar-day mean values. We found that the results are insensitive to the choice of the number of harmonics to define the seasonal cycle. The unit of eddy heat flux is converted to W m⁻² by multiplying the specific heat of the gas at constant pressure and the DJF climatological air density.

For convective heating, the daily mean data with the same horizontal and vertical resolution are derived from the Japanese 55-year Reanalysis dataset (JRA-55; Kobayashi et al. 2015), because ERA5 does not provide convective heating as an

individual variable separated from total diabatic heating. Previous studies showed that large-scale circulation associated with the convective heating from JRA-55 bears a close resemblance to that from the ECMWF interim reanalysis (Dee et al. 2011) (e.g., Park and Lee 2019; Clark and Feldstein 2020; Gong et al. 2020). To further ensure that the choice of reanalysis dataset does not affect our conclusion, we computed the eddy heat fluxes using JRA-55 and found them nearly identical to those computed from ERA5 (online supplementary Fig. S1). We also addressed potential biases in the zonal gradient of reanalysis diabatic heating by comparing it with the Global Precipitation Climatology Project data (GPCP; Huffman et al. 2001) which will be discussed in the result section.

In some of the previous climate modeling studies, the latitudinal temperature profile is represented by the Legendre polynomials that are a set of orthogonal functions (e.g., North 1975; Held and Hou 1980; Merlis and Henry 2018). By using the Legendre polynomial expansion, the zonal-mean temperature can be expressed as

$$T(\theta) = \sum_{n} a_n P_n(\sin \theta),$$

where θ is latitude, P_n is the *n*th-order Legendre polynomial, a_n is the nth-order Legendre polynomial coefficient of the zonalmean temperature. The temperature difference between equator and pole can be estimated by a_2 (i.e., the second-order Legendre polynomial coefficient) multiplied by 1.5. Applying the Legendre polynomial expansion to the daily mean temperature data, we obtain a daily time series of a_2 . We multiply -1.5to the resultant time series so that positive values correspond to enhanced equator-to-pole temperature gradients. To construct an index that measures the daily variability of a_2 , we derive a daily a_2 anomaly by removing its seasonal cycle. This time series is normalized by its DJF standard deviation and mean. The resulting time series is referred to as the $T_{\rm v}$ index; the $T_{\rm v,300}$ and $T_{v,2m}$ indices represent the equator-to-pole temperature gradient at 300 hPa and 2 m, respectively. A composite analysis with the anomalously large T_v index values demonstrates that our T_v indices capture the intended meridional temperature gradients (Figs. 1a-d).

An index that quantifies the zonal asymmetry in tropical convective heating is defined as the difference between the western and the eastern domains of tropical convective heating (Q_x) :

$$Q_x = Q_{\text{west}} - Q_{\text{east}},$$

where $Q_{\rm west}$ and $Q_{\rm east}$ are the area-weighted tropical convective heating averaged over the western (30°S–30°N, 120°E–180°) and eastern (30°S–30°N, 70°–177.5°W) tropical Pacific, following Clark and Lee (2019). The Q_x anomaly is derived by removing its seasonal cycle and then normalized by its DJF standard deviation. We refer to this normalized time series as the Q_x index hereafter. Figures 1e and f show the variability of the zonal convective heating gradient captured by this Q_x index.

We found that the $T_{y,2m}$ index exhibits an e-folding time of about 7 days, while that of the $T_{y,300}$ index is 5 days and that of the Q_x index is 4 days (supplementary Fig. S2). This indicates that all three indices grow and decay exponentially

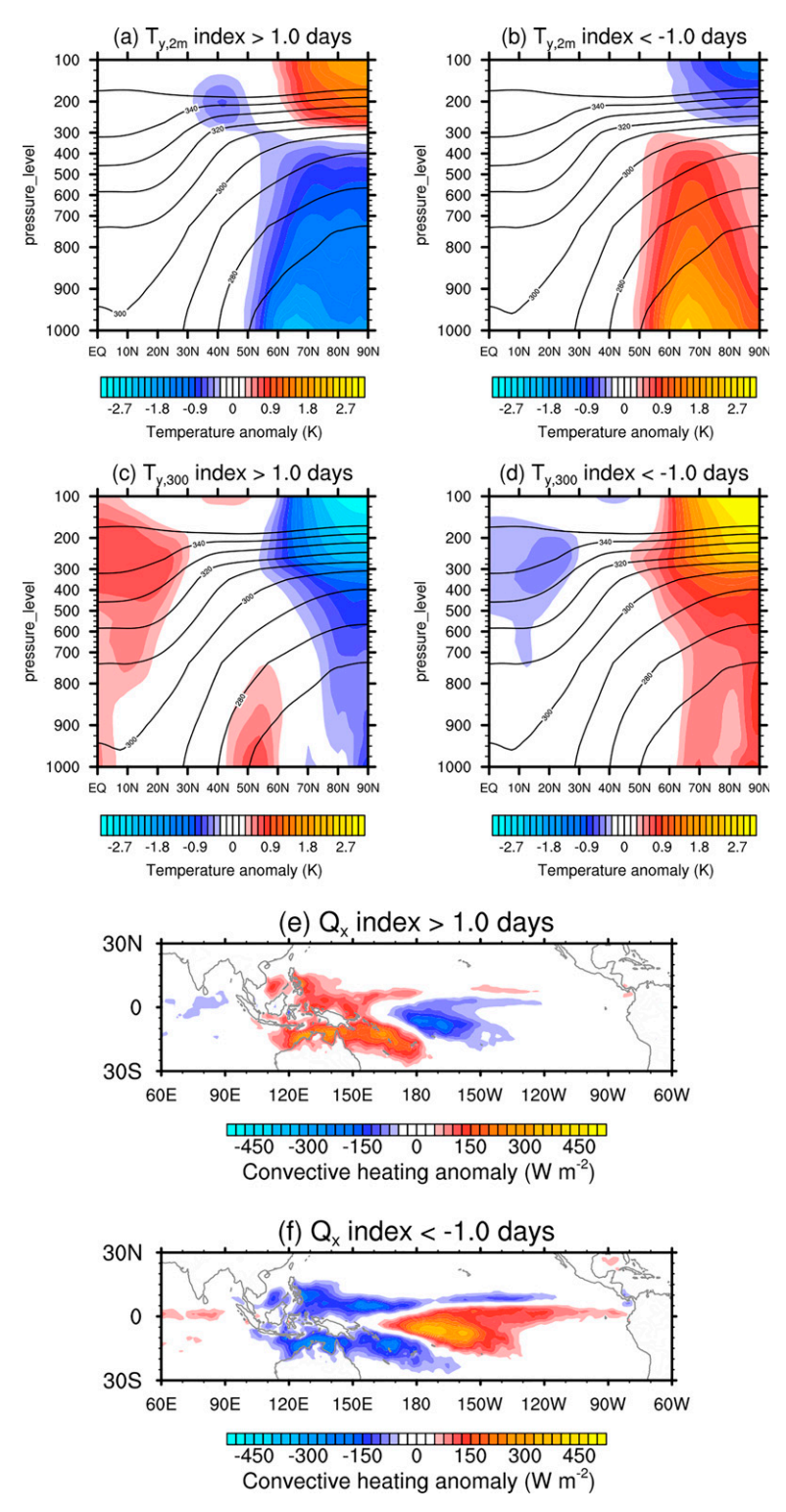


FIG. 1. (a)–(d) Zonal-mean composites of temperature anomalies during (a) the $T_{y,2\mathrm{m}}$ index > 1.0 day, (b) the $T_{y,2\mathrm{m}}$ index < -1.0 day, (c) the $T_{y,300}$ index > 1.0 day, and (d) the $T_{y,300}$ index < -1.0 day. Black lines indicate the climatological isentropic surfaces with an interval of 10 K, ranging from 270 to 350 K. (e),(f) Composites of the JRA-55 vertically integrated convective heating anomalies during (e) the Q_x index > 1.0 day and (f) the Q_x index < -1.0 day.

within one week. For the statistical significance test of the regression coefficients in Figs. 2–4, a two-sided nonparametric permutation test has been employed where random samples are drawn without replacement (Wilks 2011). A *p* value of regression coefficient is computed from a null distribution constructed by 1000 random samples for regression maps (Figs. 2 and 3) and 10000 random samples for time series (Fig. 4).

Relationships between poleward eddy heat flux and meridional temperature gradients and between poleward eddy heat flux and zonal convective heating gradient

We begin our analysis by examining latitude–pressure cross sections of eddy heat fluxes regressed against each of the three indices. Figure 2 shows the regression cross sections of daily PF anomalies onto the $T_{y,2m}$ index (top), the $T_{y,300}$ index (middle), and the Q_x index (bottom) for the recent 40 boreal winters (i.e., 1979/80–2018/19, DJF). The results do not change qualitatively but the anomalies are stronger if the recent 25 winters (i.e., 1994/95–2018/19, DJF) are used instead (not shown). For PF, we show regression coefficients at lag days -7, 0, and +7, and for SF, regression coefficients at lag days are chosen based on at which lag day the local extremum of a domain-average regression coefficient occurs (Fig. 4).

For the surface meridional temperature gradients, we find that negative PF regressions at lag days -7 to 0 precede the local temperature gradient extremum at lag day 0 (Figs. 2a,b). This indicates that negative (positive) PF anomalies precede an enhanced (suppressed) temperature gradient. As shown in Figs. 1a and 1b, these temperature gradient changes owe their existence to anomalous warming or cooling over the Arctic. This finding indicates that on the intraseasonal time scale, enhancements of the surface meridional temperature gradient are contingent upon anomalously weak PF, and vice versa. In the former case, following the enhanced temperature gradient, PF increases (Fig. 2c), but the amplitude of this positive PF anomaly is much less than that of the negative PF anomaly that led to the local temperature gradient maximum in the first place. This result is consistent with the finding by Baggett and Lee (2015) that a typical growth of PF is not contingent upon any prior condition of enhanced zonal available potential energy (ZAPE), but that the PF growth leaves behind a state of depleted ZAPE which translates into a weakened meridional temperature gradient. Therefore, conversely, if PF is suppressed, meridional temperature gradient must be anomalously strong.

The PF also appears to regulate the upper-level meridional temperature gradient, because once again PF is anomalously negative ahead of an increase of the $T_{y,300}$ index (Figs. 2d,e). However, this negative relationship is weaker than that for the surface temperature gradient and persists for a shorter time period. This behavior will be revisited later with regard to Fig. 4. Following the enhanced upper-level temperature gradient, PF is substantially enhanced throughout the extratropical troposphere poleward of 50°N (Fig. 2f).

PF anomalies are regulated by the zonal asymmetry in tropical convective heating; negative regressions indicate that extratropical PF anomalies are mostly negative (positive) prior to an enhancement (suppression) of the Q_x index (Fig. 2g). But by lag day 0, in case of the enhanced Q_x index, PF anomalies turn to mostly positive except in the limited region between 40° and 60° N (Fig. 2h). By lag day 7, extratropical PF anomalies are firmly positive (Fig. 2i). The opposite relations are drawn if the Q_x index anomalously decreases. Because it takes about one week for the Rossby waves excited in the tropics to propagate into the extratropics (Hoskins and Karoly 1981), this relatively long time delay is to be expected.

The same lag regression analysis is performed on SF anomalies (Fig. 3; note that the range of color bar is reduced by half). We see that an enhanced surface temperature gradient leads a growth of SF anomalies (Figs. 3b,c), and this growth wins the weak negative SF anomalies present in the negative lags. As a result, in contrast to the PF anomalies, the net SF anomaly is overall positive when averaged over the eddy time scale (e.g., lag -7 to +7 days; not shown), as in the baroclinic life cycle studies (Simmons and Hoskins 1978; Thorncroft et al. 1993). However, different SF behavior is found for the upper-level temperature gradient in that the local temperature gradient maximum tends to be preceded by negative midlatitude SF anomalies (Fig. 3d). SF anomalies poleward of 60°N start grow in the upper troposphere on lag day 0 (Figs. 3d,e), but this SF growth is weaker than that associated with the surface temperature gradient (Fig. 3f). The regressions against the Q_x index show that weakly positive SF anomalies in the tropics precede the enhanced zonal asymmetry of convective heating (Figs. 3g,h). However, negative SF anomalies become prominent in the midlatitude within a week (not shown). We note that the signs of SF anomalies are opposite in the above discussion in case of the negative index value at lag day 0.

We tested the sensitivity of the regression results to the definition of the temperature gradient. The alternative definition that we used is the tropical average (15°S–15°N) minus the high-latitude average (60°–90°N) temperature. It turned out that the aforementioned lead–lag relationships hold, with stronger magnitudes across all lag days (supplementary Figs. S3 and S4).

The results thus far show that the eddy flux-temperature/heating gradient relationships show significant temporal variations. Therefore, we examine the time series of regression coefficients between the three indices and the domain-averaged tropospheric eddy heat fluxes from lag -20 to +20 days. The domain (i.e., 30° - 80° N, 300-1000 hPa) of the tropospheric eddy heat flux is chosen based on the structure of the climatological eddy heat fluxes (supplementary Fig. S1) and the regression fields (Figs. 2 and 3). We found that our conclusions are insensitive to the choice of eddy heat flux domain (e.g., 20° - 90° N, 30° - 70° N, and 50° - 90° N).

In the negative lags, PF anomalies are negatively correlated with all three indices (Figs. 4a,c,e), with the strongest relationship in the surface temperature gradient. With respect to the surface temperature gradient, PF minimum peaks at lag day -5 (Fig. 4a). A day later, at lag day -4, SF starts to increase (Fig. 4b). PF regression coefficients turn positive in the positive lags, but with much smaller magnitudes than the

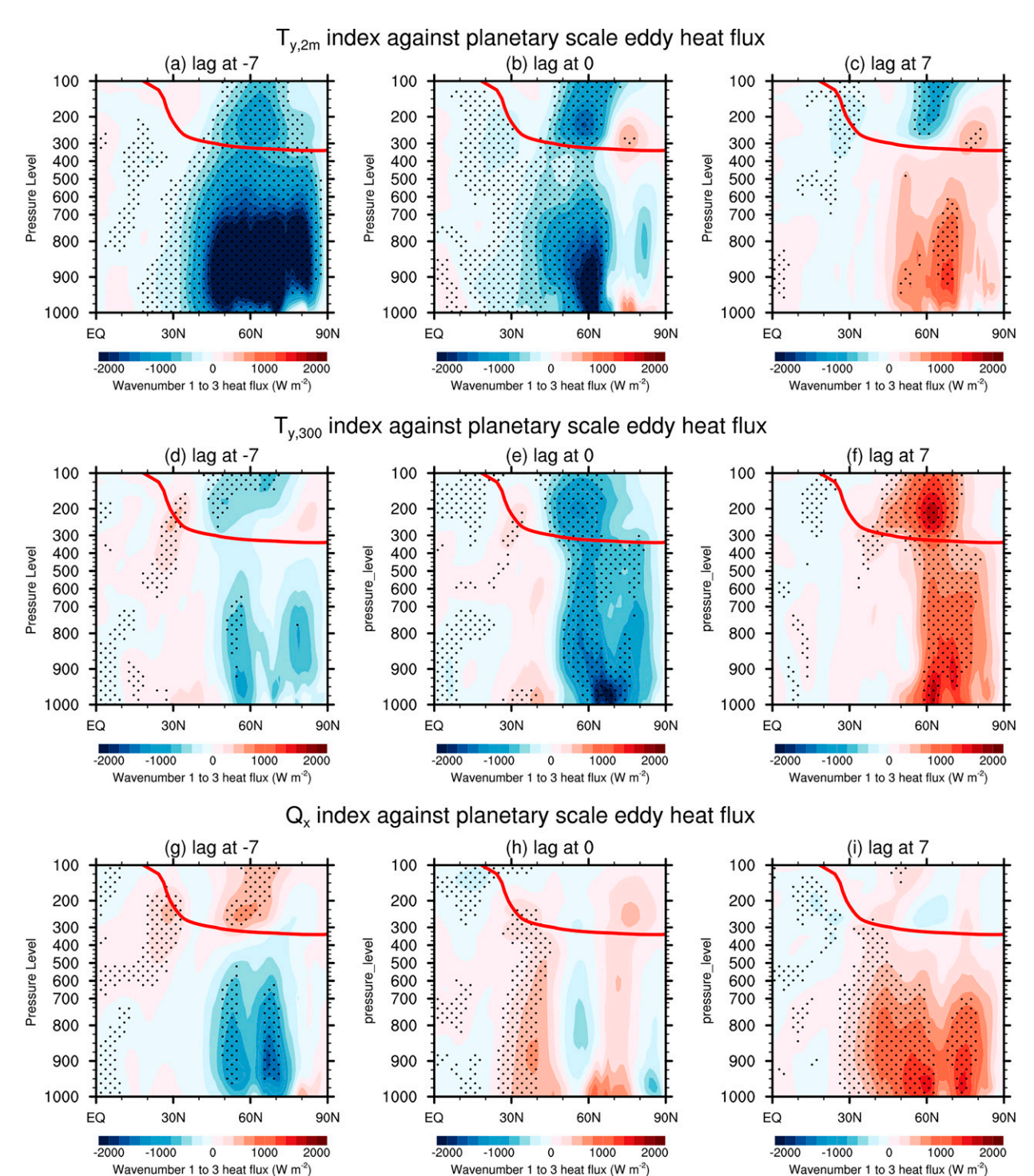


Fig. 2. Lag-regression maps of planetary-scale (k = 1-3) eddy heat flux onto (top) the $T_{y,2m}$ index, (middle) the $T_{y,300}$ index, and (bottom) the Q_x index during 1979/80–2018/19, DJF, at (a),(d),(g) lag day -7, (b),(e),(h) lag day 0, and (c),(f),(i) lag day +7. Stippling indicates the 1% significance level and correlation value larger than 0.05. Statistical significance is evaluated by a two-sided permutation test with 1000 random samples. The 2-PVU isoline is denoted by a red contour in each panel.

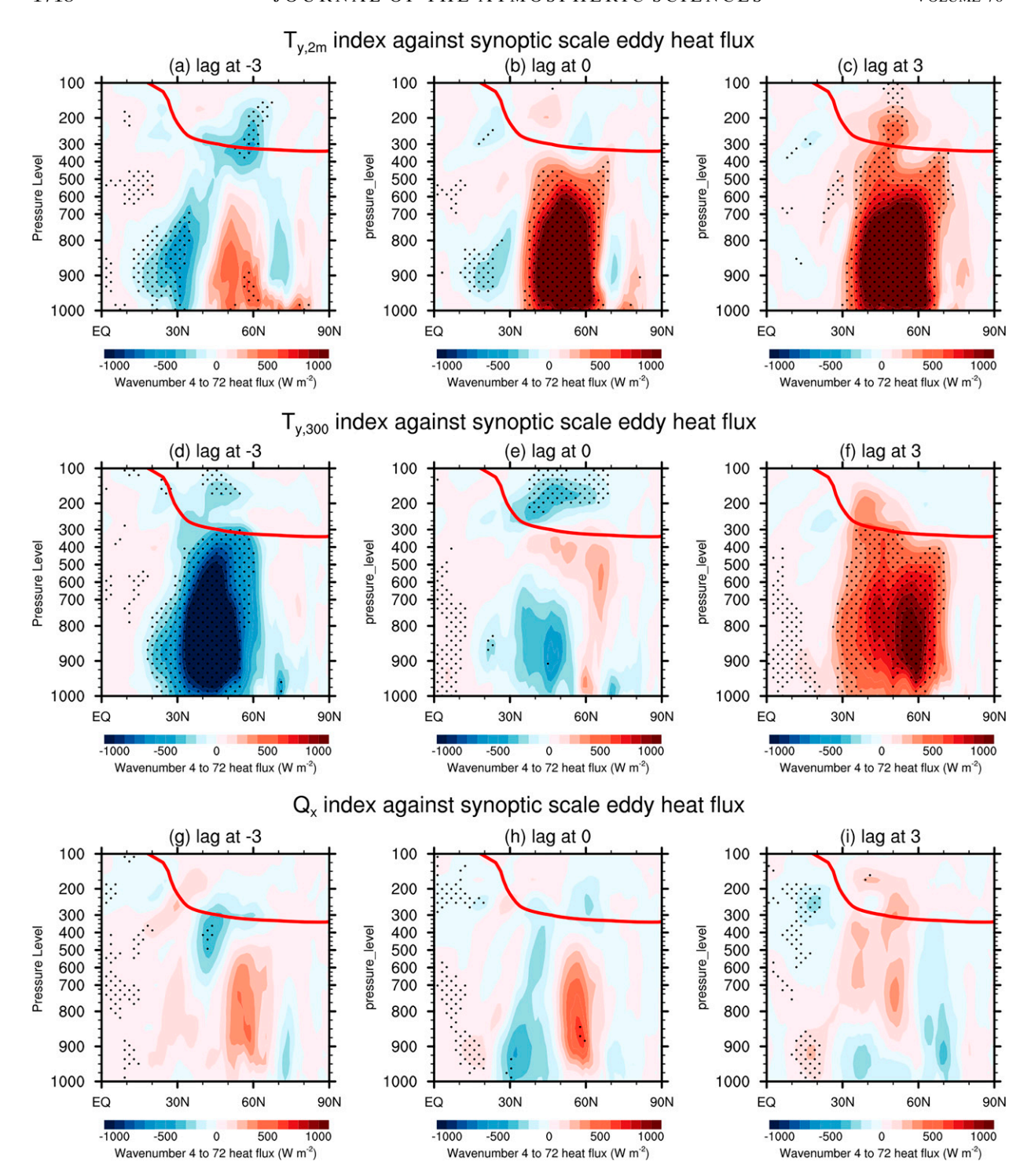


FIG. 3. As in Fig. 2, but for synoptic-scale (k = 4-72) eddy heat flux at (a),(d),(g) lag day -3, (b),(e),(h) lag day 0, and (c),(f),(i) lag day +3. For visualization, the range of the color bar is reduced by half from that in Fig. 2.

negative values in the negative lags. These lead–lag relationships indicate that the surface temperature gradient variability is regulated by planetary-scale eddies. This finding is consistent with previous studies that examined relationships between eddy heat fluxes and the tropospheric isentropic slope which is proportional

to the meridional temperature gradient (Thompson and Birner 2012; Park and Lee 2021). In Figs. 4a and 4b, if integrated over lag days, PF and SF regressions oppose each other. This result is also consistent with previous findings that during boreal winter stationary and transient eddy energy fluxes oppose each other

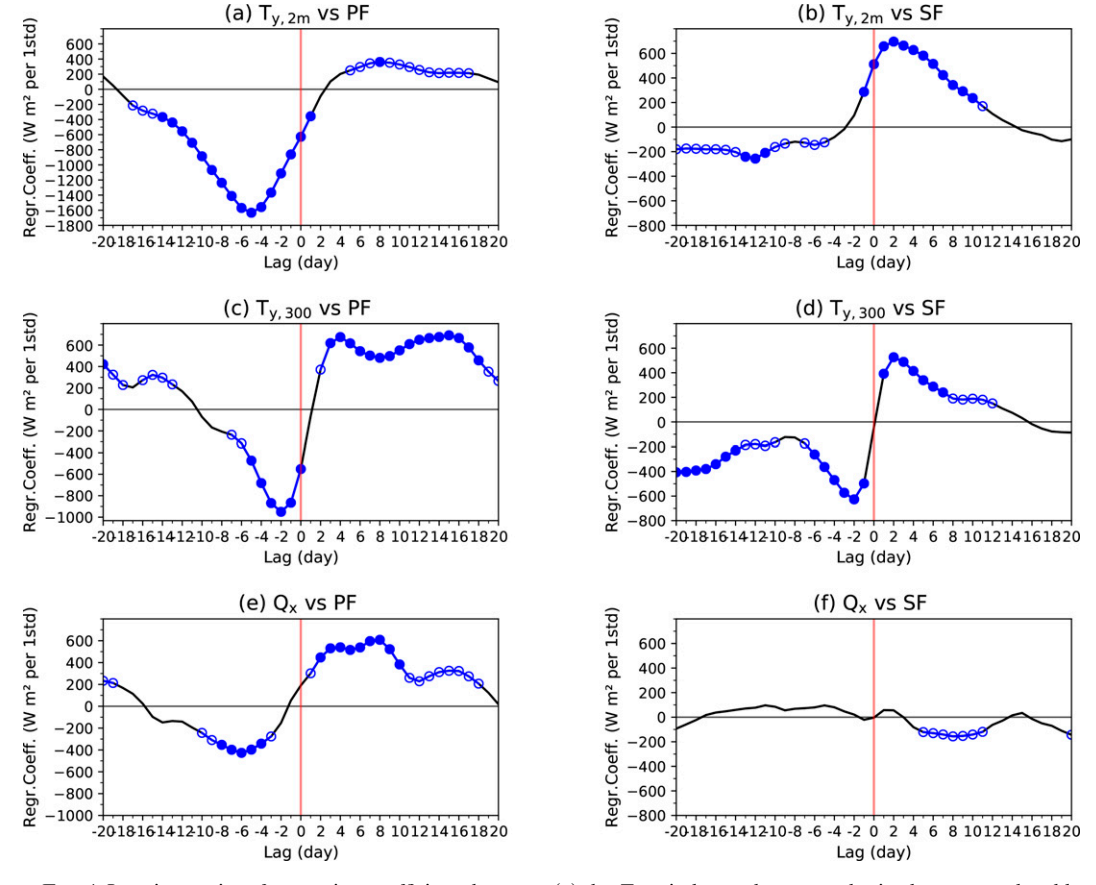


FIG. 4. Lag time series of regression coefficients between (a) the $T_{y,2m}$ index vs the tropospheric planetary-scale eddy heat flux and that between (b) the $T_{y,2m}$ index and the tropospheric synoptic-scale eddy heat flux for 1979/80–2018/19 DJF days. (c)–(f) As in (a) and (b), but regressed against (c),(d) the $T_{y,300}$ index and (e),(f) the Q_x index. Filled circles indicate the 0.1% significance level, while open circles indicate the 5% significance level. Statistical significance is evaluated by a two-sided permutation test with 10 000 random samples.

(Trenberth and Stepaniak 2003; Kaspi and Schneider 2013; Barpanda and Shaw 2017; Shaw et al. 2018). This compensation between PF and SF (or stationary and transient eddy heat fluxes) may help explain why the correlation between the eddy heat flux and meridional temperature gradient is smaller in the Northern Hemisphere (NH) than that in the Southern Hemisphere (Chemke and Polvani 2020).

For the upper-tropospheric temperature gradient, the evolution of PF and SF anomalies are more symmetric about lag day 0 in the sense that negative heat flux anomalies appear in the negative lags and positive heat flux anomalies prevail in the positive lags (Figs. 4c,d). This time evolution indicates that the temperature gradient is enhanced if these heat fluxes are anomalously weak, and in turn the enhanced temperature gradient promotes the growth of the heat fluxes. This lead–lag relationship is to be expected from the flux–gradient relationship. However, the growth of the SF anomalies in the positive lags is weaker than that associated with the surface temperature gradient (Fig. 4b), indicating that SF is more sensitive to the surface temperature gradient. This SF sensitivity to the surface temperature gradient is

consistent with the finding from a recent idealized modeling study (Yuval and Kaspi 2020).

For the zonal gradient of tropical convective heating, both PF and SF are rather asymmetric with respect to the Q_x index: the Q_x index extremum is preceded by negative PF anomalies (Fig. 4e), but they are notably smaller in magnitude than the positive PF anomalies that follow in the positive lags; the SF anomalies show more striking asymmetry in that significant anomalies are present only in the positive lags, and the anomalies are negative, suggesting that SF declines in response to an enhanced Q. The time sequence that positive PF anomaly precedes negative SF anomaly can be understood from the relationships between the surface temperature gradients and eddy heat fluxes (Figs. 4a,b); positive PF anomaly reduces the meridional temperature gradient, which is ensued by negative SF anomaly. The time sequence of positive Q_x anomaly \rightarrow positive PF anomaly → negative SF anomaly is in line with a recent finding that enhanced zonal gradient in tropical convection during the preceding December contributes to a hemispherewide suppression of extratropical storm tracks during January (Park and Lee 2020).

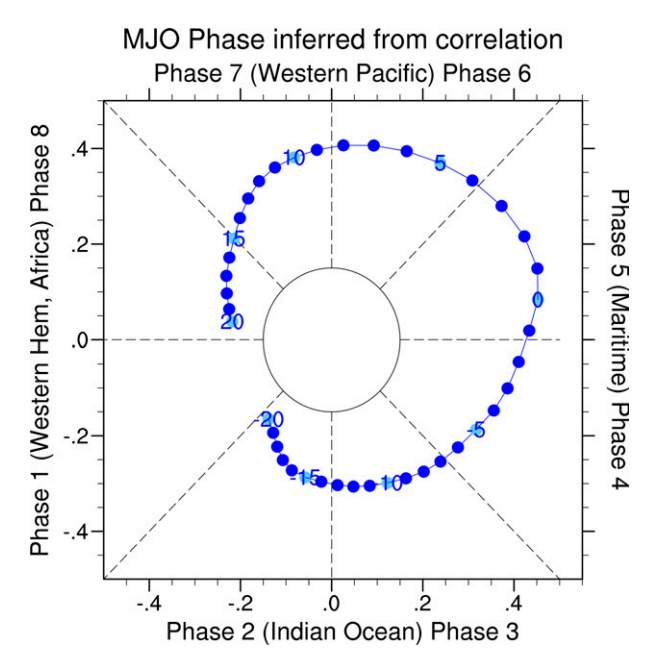


FIG. 5. MJO phase-space diagram based on lag correlation between the Q_x index and the RMM indices. Each circle denotes correlation values at each lag day, and 5-day labels are overlaid on phase line.

That PF is anomalously weak ahead of the Q_x index maximum raises an interesting question because, unlike for the meridional temperature gradients, there is no obvious reason as to why extratropical PF anomaly might influence the zonal gradient of tropical convection. Based on the 30-40-day periodicity evident in Fig. 4e, we hypothesize that the behavior of the PF regression coefficients in part reflects the influence of Madden-Julian oscillation (MJO; Madden and Julian 1971) variability. To examine this possibility, we perform a lag correlation analysis of the realtime multivariate MJO (RMM; Wheeler and Hendon 2004) indices against the Q_r index. The result shows the presence of phase 1 (suppressed Q_x) at lag day -20 and phase 5 (enhanced Q_x) at lag day -1 (Fig. 5). This finding that the MJO regulates the Q_x variability and the subsequent poleward heat flux is consistent with the result of Lee and Yoo (2014). Thus, we conclude that the anomalously weak PF anomaly in the negative lags reflects the PF response to MJO phase 1 which produces more zonally uniform convective heating.

Lag correlations corresponding to the lag regressions in Fig. 4 show the largest correlation (r = -0.3) when PF is correlated with the $T_{y,2\mathrm{m}}$ index (supplementary Fig. S5). This finding reveals that approximately 9% of the variance in the surface equator-to-pole temperature gradient is explained by PF variability.

From these analyses, we draw three conclusions about eddy heat fluxes in the NH during DJF. First, it is the $T_{y,300}$ index and the Q_x index that result in the enhancement of the extratropical PF anomalies (Figs. 4c,e). Second, an enhancement in the surface meridional temperature gradient is contingent upon suppressed PF anomalies (Fig. 4a) and, as expected from the flux–gradient relationship for baroclinic waves, SF grows

following the anomalously strong surface temperature gradient.¹ Third, an enhancement in the upper-tropospheric meridional temperature gradient occurs if PF and/or SF are anomalously weak (Figs. 4c,d). The net effect of the upper-level baroclinity on positive SF anomalies is weaker than that of the surface baroclinity (Figs. 3c,f and 4b,d).

While the results hitherto describe the relationships between eddy heat fluxes and each index, these indices are not necessarily independent of each other. Therefore, we examine if the three indices are correlated with each other (supplementary Fig. S6). It is shown that both the Q_x and $T_{v,300}$ indices precede the $T_{v,2m}$ index by a few days, and there is a 30-40-day periodicity. The periodicity, together with the presence of the MJO phase propagation associated with the Q_x index (Fig. 5), suggests that the MJO plays an important role in connecting the variability of the temperature gradients to the Q_x index. In fact, Lee and Yoo (2014) examined temperature variability associated with the MJO and found that an increase/decrease of the upper-tropospheric temperature gradient precedes an increase/decrease of the surface temperature gradient by a few days (their Fig. 2). As discussed earlier, both the Q_x index and the $T_{y,300}$ index lead the anomalous growth/decay of extratropical PF by a few days (Figs. 4c,e), which modulates the surface temperature gradient. Thus, the time sequence of enhanced zonal heating asymmetry and upper-level temperature gradient → positive PF anomaly → negative surface temperature gradient, or vice versa, can be in part explained by the MJO variability.

4. Trends of the meridional temperature gradients, zonal convective heating gradient, and eddy heat fluxes

Returning to the topic of the temperature gradient trends raised in the introduction, we examine the time series of the seasonally averaged three indices (Fig. 6) and temperature anomalies over the tropics and the polar region (Fig. 7) for the past 40 winters. We see that the $T_{y,2m}$ index has indeed been declining (Fig. 6a), but there is no trend in the $T_{v,300}$ index (Fig. 6b) according to a nonparametric Mann-Kendall trend test (Mann 1945). This second result owes to the fact that the warming rate in the polar upper troposphere (0.3 K decade⁻¹; Fig. 7b) is as strong as that in the tropical upper troposphere $(0.2 \text{ K decade}^{-1};$ Fig. 7d). Consistent with the trends of the P_2 indices, the time series of the temperature difference between the polar region and the tropics at the upper troposphere shows no trend (Fig. 7f), while that at the surface reveals a strong declining trend (Fig. 7e). The muted upper-tropospheric temperature trend is at odds with the climate model predictions. This discrepancy could be attributed to internal variability in nature or uncertainties in observation data (Santer et al. 2017; Suárez-Gutiérrez et al. 2017), but also to the too aggressive warming of tropical upper troposphere (Fu et al. 2011; McKitrick and Christy 2020; Mitchell et al. 2013; Bao et al. 2021) and not enough warming in the

¹ Figure 4a shows positive PF regression values in the positive lags, implying that some of the PF also follow the flux-gradient relationship. However, the negative PF values in the negative lags are far greater than the positive values, and the former cannot be explained by the flux-gradient relationship.

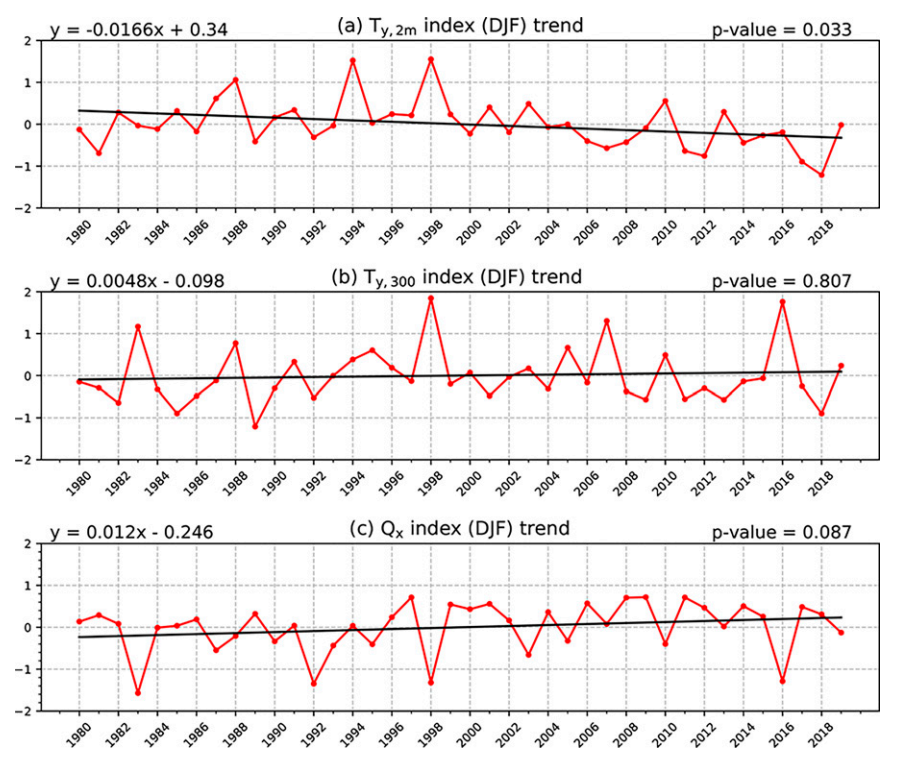


FIG. 6. Time series of the DJF-mean (a) $T_{y,2\mathrm{m}}$ index, (b) $T_{y,300}$ index, and (c) Q_x index for 1979/80–2018/19, with the convention that the starting year 1980 refers to the 1979/80 DJF. A least squares linear regression line indicates the linear trend, and its slope and intercept are displayed at the upper-left corner. The p values of the interdecadal trends are evaluated by a Mann–Kendall trend test.

Arctic upper troposphere (Cohen et al. 2020) in models. Regardless, we find that the "tug-of-war" has not been occurring in nature, at least over the analysis period.

Instead, the zonal asymmetry of tropical convective heating, which is shown to be effective at promoting PF into the Arctic, has been gradually intensifying (Fig. 6c). This result is corroborated by other recent findings that the tropical Pacific zonal SST gradient has been increasing over the past several decades (Chung et al. 2019; Clark and Lee 2019; Seager et al. 2019; Johnson et al. 2020), and by outgoing longwave radiation over the recent 40 winters (not shown).

This reanalysis-based Q_x trend is compared with the GPCP precipitation trend. Chemke and Polvani (2019) showed that in the 1979–2010 period, the trends in reanalysis latent heating are much stronger than the GPCP precipitation trends over the tropics. Therefore, we investigate if the zonal distribution trend of the GPCP precipitation is consistent with that of the JRA-55 convective heating and also the ERA5 precipitation (supplementary Fig. S7). We found that in all three datasets, the zonal gradients of the heating/precipitation have been increasing. Over the domain of the Q_x index (30°S–30°N, 120°E–70°W), the pattern correlation between the GPCP and the ERA5 precipitation trends is 0.81 and that between the GPCP and the JRA-55 heating trends is 0.63. To ascertain the sensitivity of the results derived from the Q_x index, we further examined the regression

of eddy heat fluxes against an alternative Q_x index constructed using the GPCP. As shown in supplementary Fig. S8, we again found that both PF and SF regressions using the GPCP-based Q_x index are qualitatively consistent with those using the JRA-55 heating. Therefore, we conclude that the qualitative results of this study are insensitive to the choice of data for the Q_x index.

Given the relationships between the eddy heat fluxes and the Q_x and $T_{y,2m}$ indices, the fact that these indices show significant trends suggests that eddy heat fluxes also underwent significant trends (Fig. 8). We see that trends in total eddy heat flux (TF) display positive signs at the subtropical upper troposphere and the 30°-50°N latitudinal band, whereas negative signs are prominent in the 50°-80°N band at the lower troposphere (Fig. 8a). Moreover, Figs. 8b and 8c show that the SF trends account for the dipole meridional structure in the TF trends, whereas the PF trends tend to negate the TF trends. The weakening lowertropospheric SF trends are consistent with previous findings (e.g., Chemke and Polvani 2020; Yuval and Kaspi 2020) and conform to the flux-gradient relationship. However, the same flux-gradient relationship cannot explain the increasing PF trends. Indeed, Park and Lee (2021) showed that localized tropical heating anomalies can drive extratropical PF anomalies and regulate the extratropical isentropes that subsequently suppress SF anomalies. Caution is still warranted, however, because the eddy heat flux variability on longer time scales could be also

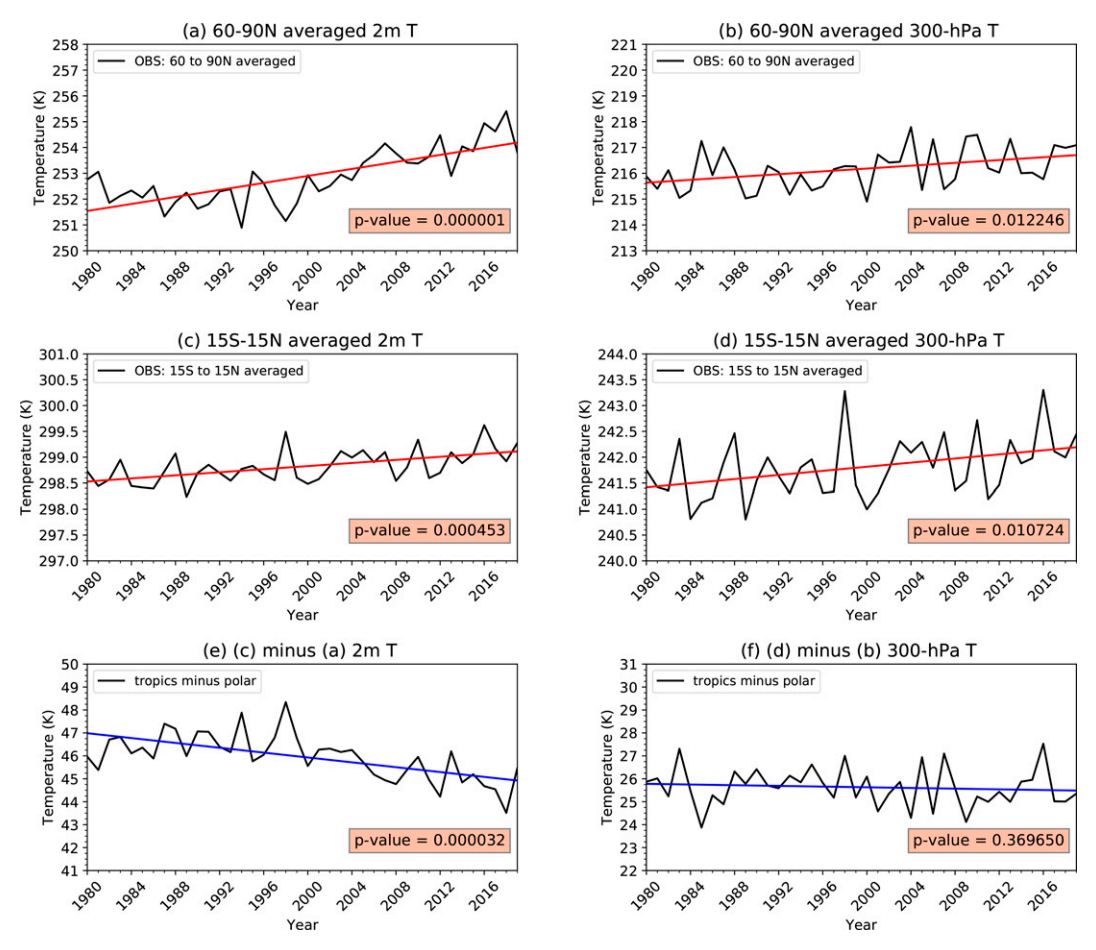


FIG. 7. Time series of the cosine-weighted zonal-mean temperature anomalies averaged over 60° – 90° N at (a) the surface (i.e., 2 m) and (b) 300 hPa for 1979/80 to 2018/19, DJF, with the convention that the starting year 1980 refers to the 1979/80 DJF. (c),(d) As in (a) and (b), but averaged over 15°S–15°N. (e),(f) Time series of difference between (c) and (a) and between (d) and (b), respectively. Red and blue lines indicate positive and negative linear trends, respectively. The p values of the interdecadal trends are evaluated by a Mann–Kendall trend test.

affected by orography or transient eddy forcing (Held et al. 1989, 2002). Such linkages on the interdecadal time scale will be further investigated in a future study.

5. Discussion and conclusions

In this study, using reanalysis data, we examined how eddy heat fluxes are related to the upper-tropospheric and surface meridional temperature gradients, and to the zonal gradient of tropical convective heating. Key findings are summarized as follows: First, on time scales of baroclinic eddy life cycles, the surface temperature gradient anomalies are regulated by planetary-scale eddy heat flux, while synoptic-scale eddy heat flux responds to variations in the surface temperature gradient. These relationships are consistent with the findings in previous studies that separated eddy activities by length scales (Baggett and Lee 2015; Graversen and Burtu 2016; Park and Lee 2021) and by time scales (Thompson and Birner 2012). Second, with respect to the upper-tropospheric temperature gradient, both PF and SF follow the flux–gradient relationship, and PF variability is greater than

SF variability. Last, we found that the zonal asymmetry of tropical convective heating is also influential in driving positive PF anomalies in the extratropics. This positive PF anomaly reduces meridional temperature gradient especially at the surface, leading to suppressed SF anomalies. These physical processes suggest that the upward trending heating asymmetry (Fig. 7c) has contributed to the declining surface temperature gradient (Fig. 7a).

As a way to further explore this possibility, we computed the correlation between the DJF-mean Q_x index and the $T_{y,2\mathrm{m}}$ index (supplementary Fig. S9). The result reveals that they are negatively correlated (r=-0.319, p=0.045). If we remove four outliers that correspond to particularly strong El Niño years, the relation becomes even stronger (r=-0.402, p=0.015). This result indicates that during winters of enhanced zonal heating asymmetry, the surface meridional temperature gradient tends to be suppressed. The implication is that the intraseasonal-time-scale relationship between Q_x and $T_{y,2\mathrm{m}}$ is manifested also on the interannual time scale.

By examining daily time-scale variability, we show evidence that SF responds to PF variations. In the context of the

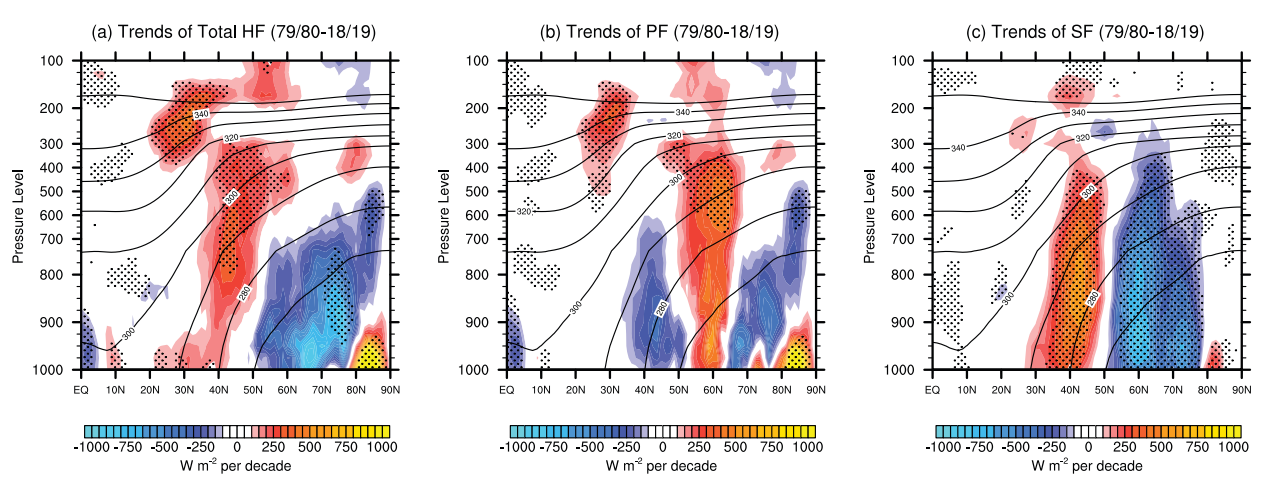


FIG. 8. Trend map of the DJF-mean (a) total eddy heat flux (b) planetary-scale eddy heat flux, and (c) synoptic-scale eddy heat flux anomalies for 1979/80–2018/19. Stippling indicates a statistical significance at the 10% level evaluated by a Mann–Kendall trend test, while black lines indicate the climatological isentropic surfaces with an interval of 10 K, ranging from 270 to 350 K.

atmospheric energy transport, prior studies have shown similar compensations, but between stationary and transient eddy fluxes (e.g., Trenberth and Stepaniak 2003; Kaspi and Schneider 2013; Barpanda and Shaw 2017; Shaw et al. 2018). For example, employing a moist static energy (MSE) framework, Barpanda and Shaw (2017) showed that compensation between stationary and transient eddy energy fluxes occurs on time scales from seasonal to centennial time scales.

More recently, Shaw and Graham (2020) showed in their snowball Earth simulations that transient eddy MSE flux is more strongly correlated with surface moisture gradient, rather than surface or lower-tropospheric temperature gradient. Thus, the eddy interactions are not just mediated by the meridional temperature gradients. Nevertheless, the results of this study point out that attention should be given to the *zonal* convective heating gradient as much as to the meridional temperature gradients.

Acknowledgments. We acknowledge the three anonymous reviewers for their helpful comments and suggestions. We thank Steven B. Feldstein, Changhyun Yoo, and Dong Wan Kim for their helpful discussion. This study was supported by NSF OPP-1723832, AGS-1822015, and AGS-1948667.

Data availability statement. The ERA5 data used in this study can be downloaded from the Copernicus Climate Change Service Climate Data Store (https://cds.climate.copernicus.eu/). The JRA-55 data and the GPCP data can be downloaded from the Research Data Archive at the National Center for Atmospheric Research (https://rda.ucar.edu).

REFERENCES

Baggett, C., and S. Lee, 2015: Arctic warming induced by tropically forced tapping of available potential energy and the role of the planetary-scale waves. J. Atmos. Sci., **72**, 1562–1568, https://doi.org/10.1175/JAS-D-14-0334.1.

Bao, J., B. Stevens, L. Kluft, and D. Jiménez-de-la-Cuesta, 2021: Changes in the tropical lapse rate due to entrainment and their impact on climate sensitivity. *Geophys. Res. Lett.*, 48, e2021GL094969, https://doi.org/10.1029/2021GL094969.

Barnes, E. A., and L. M. Polvani, 2015: CMIP5 projections of Arctic amplification, of the North American/North Atlantic circulation, and of their relationship. *J. Climate*, 28, 5254–5271, https:// doi.org/10.1175/JCLI-D-14-00589.1.

Barpanda, P., and T. Shaw, 2017: Using the moist static energy budget to understand storm-track shifts across a range of time scales. J. Atmos. Sci., 74, 2427–2446, https://doi.org/10. 1175/JAS-D-17-0022.1.

Butler, A. H., D. W. J. Thompson, and R. Heikes, 2010: The steady-state atmospheric circulation response to climate change-like thermal forcings in a simple general circulation model. J. Climate, 23, 3474–3496, https://doi.org/10.1175/ 2010JCLI3228.1.

Cattiaux, J., and C. Cassou, 2013: Opposite CMIP3/CMIP5 trends in the wintertime northern annular mode explained by combined local sea ice and remote tropical influences. *Geophys. Res. Lett.*, 40, 3682–3687, https://doi.org/10.1002/grl.50643.

Chemke, R., and L. M. Polvani, 2019: Opposite tropical circulation trends in climate models and in reanalyses. *Nat. Geosci.*, 12, 528–532, https://doi.org/10.1038/s41561-019-0383-x.

—, and —, 2020: Linking midlatitudes eddy heat flux trends and polar amplification. *npj Climate Atmos. Sci.*, **3**, 8, https://doi.org/10.1038/s41612-020-0111-7.

Chung, E.-S., A. Timmermann, B. J. Soden, K.-J. Ha, L. Shi, and V. O. John, 2019: Reconciling opposing Walker circulation trends in observations and model projections. *Nat. Climate Change*, 9, 405–412, https://doi.org/10.1038/s41558-019-0446-4.

Clark, J. P., and S. Lee, 2019: The role of the tropically excited Arctic warming mechanism on the warm Arctic cold continent surface air temperature trend pattern. *Geophys. Res. Lett.*, 46, 8490–8499, https://doi.org/10.1029/2019GL082714.

—, and S. B. Feldstein, 2020: What drives the North Atlantic Oscillation's temperature anomaly pattern? Part II: A

- decomposition of the surface downward longwave radiation anomalies. *J. Atmos. Sci.*, **77**, 199–216, https://doi.org/10.1175/JAS-D-19-0028.1.
- Cohen, J., and Coauthors, 2020: Divergent consensuses on Arctic amplification influence on midlatitude severe winter weather. *Nat. Climate Change*, **10**, 20–29, https://doi.org/10.1038/s41558-019-0662-y.
- Dee, D. P., and Coauthors, 2011: The ERA-Interim reanalysis: Configuration and performance of the data assimilation system. *Quart. J. Roy. Meteor. Soc.*, **137**, 553–597, https://doi.org/10.1002/qj.828.
- Franchito, S. H., and V. B. Rao, 2003: The correlation between temperature gradient and eddy heat flux in the Northern and Southern Hemispheres. *J. Meteor. Soc. Japan*, **81**, 163–168, https://doi.org/10.2151/jmsj.81.163.
- Fu, Q., S. Manabe, and C. M. Johanson, 2011: On the warming in the tropical upper troposphere: Models versus observations. *Geophys. Res. Lett.*, 38, L15704, https://doi.org/10.1029/ 2011GL048101.
- Gong, T., S. B. Feldstein, and S. Lee, 2020: Rossby wave propagation from the Arctic into the midlatitudes: Does it arise from in situ latent heating or a trans-Arctic wave train? *J. Climate*, 33, 3619–3633, https://doi.org/10.1175/JCLI-D-18-0780.1.
- Goss, M., S. B. Feldstein, and S. Lee, 2016: Stationary wave interference and its relation to tropical convection and Arctic warming. *J. Climate*, 29, 1369–1389, https://doi.org/10.1175/JCLI-D-15-0267.1.
- Graversen, R. G., and M. Burtu, 2016: Arctic amplification enhanced by latent energy transport of atmospheric planetary waves. *Quart. J. Roy. Meteor. Soc.*, **142**, 2046–2054, https:// doi.org/10.1002/qj.2802.
- Green, J. S. A., 1970: Transfer properties of the large-scale eddies and the general circulation of the atmosphere. *Quart. J. Roy. Meteor. Soc.*, **96**, 157–185, https://doi.org/10.1002/qj.49709640802.
- Harvey, B. J., L. C. Shaffrey, and T. J. Woollings, 2014: Equator-to-pole temperature differences and the extra-tropical storm track responses of the CMIP5 climate models. *Climate Dyn.*, 43, 1171–1182, https://doi.org/10.1007/s00382-013-1883-9.
- Held, I. M., and A. Y. Hou, 1980: Nonlinear axially symmetric circulations in a nearly inviscid atmosphere. *J. Atmos. Sci.*, **37**, 515–533, https://doi.org/10.1175/1520-0469(1980)037<0515: NASCIA>2.0.CO;2.
- —, and E. O'Brien, 1992: Quasigeostrophic turbulence in a three-layer model: Effects of vertical structure in the mean shear. J. Atmos. Sci., 49, 1861–1870, https://doi.org/10.1175/ 1520-0469(1992)049<1861:OTIATL>2.0.CO;2.
- —, S. W. Lyons, and S. Nigam, 1989: Transients and the extratropical response to El Niño. *J. Atmos. Sci.*, **46**, 163–174, https://doi.org/10.1175/1520-0469(1989)046<0163:TATERT>2. 0 CO-2
- —, M. Ting, and H. Wang, 2002: Northern winter stationary waves: Theory and modeling. *J. Climate*, **15**, 2125–2144, https://doi.org/10.1175/1520-0442(2002)015<2125:NWSWTA> 2.0 CO-2
- Hersbach, H., and Coauthors, 2020: The ERA5 global reanalysis. *Quart. J. Roy. Meteor. Soc.*, **146**, 1999–2049, https://doi.org/10.1002/qj.3803.
- Hoskins, B., and D. Karoly, 1981: The steady linear response of a spherical atmosphere to thermal and orographic forcing. *J. Atmos. Sci.*, **38**, 1179–1196, https://doi.org/10.1175/1520-0469(1981)038<1179:TSLROA>2.0.CO;2.

- Huffman, G. J., and Coauthors, 2001: Global precipitation at one-degree daily resolution from multisatellite observations. *J. Hydrometeor.*, **2**, 36–50, https://doi.org/10.1175/1525-7541(2001) 002<0036:GPAODD>2.0.CO;2.
- Johnson, N. C., L. Krishnamurthy, A. T. Wittenberg, B. Xiang, G. A. Vecchi, S. B. Kapnick, and S. Pascale, 2020: The impact of sea surface temperature biases on North American precipitation in a high-resolution climate model. *J. Climate*, 33, 2427–2447, https://doi.org/10.1175/JCLI-D-19-0417.1.
- Kaspi, Y., and T. Schneider, 2013: The role of stationary eddies in shaping midlatitude storm tracks. J. Atmos. Sci., 70, 2596–2613, https://doi.org/10.1175/JAS-D-12-082.1.
- Kobayashi, S., and Coauthors, 2015: The JRA-55 reanalysis: General specifications and basic characteristics. *J. Meteor. Soc. Japan.* **93**, 5–48, https://doi.org/10.2151/jmsj.2015-001.
- Kushner, P. J., and I. M. Held, 1998: A test, using atmospheric data, of a method for estimating oceanic eddy diffusivity. *Geophys. Res. Lett.*, 25, 4213–4216, https://doi.org/10.1029/1998GL900142.
- Lee, S., and C. Yoo, 2014: On the causal relationship between pole-ward heat flux and the equator-to-pole temperature gradient: A cautionary tale. *J. Climate*, **27**, 6519–6525, https://doi.org/10.1175/JCLI-D-14-00236.1.
- —, T. Gong, N. Johnson, S. B. Feldstein, and D. Pollard, 2011: On the possible link between tropical convection and the Northern Hemisphere Arctic surface air temperature change between 1958 and 2001. J. Climate, 24, 4350–4367, https://doi. org/10.1175/2011JCLI4003.1.
- Lorenz, E. N., 1979: Forced and free variations of weather and climate. J. Atmos. Sci., 36, 1367–1376, https://doi.org/10.1175/ 1520-0469(1979)036<1367:FAFVOW>2.0.CO;2.
- Lunkeit, F., K. Fraedrich, and S. E. Bauer, 1998: Storm tracks in a warmer climate: Sensitivity studies with a simplified global circulation model. *Climate Dyn.*, 14, 813–826, https://doi.org/ 10.1007/s003820050257.
- Madden, R. A., and P. R. Julian, 1971: Detection of a 40–50 day oscillation in the zonal wind in the tropical Pacific. *J. Atmos. Sci.*, **28**, 702–708, https://doi.org/10.1175/1520-0469(1971)028
 0702:DOADOI>2.0.CO:2.
- Mann, H., 1945: Nonparametric tests against trend. *Econometrica*, 13, 245–259, https://doi.org/10.2307/1907187.
- McKitrick, R., and J. Christy, 2020: Pervasive warming bias in CMIP6 tropospheric layers. *Earth Space Sci.*, **7**, e2020EA001281, https://doi.org/10.1029/2020EA001281.
- Merlis, T. M., and M. Henry, 2018: Simple estimates of polar amplification in moist diffusive energy balance models. *J. Climate*, 31, 5811–5824, https://doi.org/10.1175/JCLI-D-17-0578.1.
- Mitchell, D. M., P. W. Thorne, P. A. Stott, and L. J. Gray, 2013: Revisiting the controversial issue of tropical tropospheric temperature trends. *Geophys. Res. Lett.*, 40, 2801–2806, https://doi.org/10.1002/grl.50465.
- North, G. R., 1975: Theory of energy-balance climate models. *J. Atmos. Sci.*, **32**, 2033–2043, https://doi.org/10.1175/1520-0469(1975)032<2033:TOEBCM>2.0.CO;2.
- O'Gorman, P. A., 2010: Understanding the varied response of the extratropical storm tracks to climate change. *Proc. Natl. Acad. Sci. USA*, **107**, 19176–19180, https://doi.org/10.1073/pnas.1011547107.
- Park, M., and S. Lee, 2019: Relationship between tropical and extratropical diabatic heating and their impact on stationary– transient wave interference. *J. Atmos. Sci.*, 76, 2617–2633, https://doi.org/10.1175/JAS-D-18-0371.1.
- —, and —, 2020: A mechanism for the midwinter minimum in North Pacific storm-track intensity from a global

- perspective. *Geophys. Res. Lett.*, **47**, e2019GL086052, https://doi.org/10.1029/2019GL086052.
- —, and —, 2021: The role of planetary-scale eddies on the recent isentropic slope trend during boreal winter. *J. Atmos. Sci.*, **78**, 2879–2894, https://doi.org/10.1175/JAS-D-20-0348.1.
- Pavan, V., 1996: Sensitivity of a multi-layer quasi-geostrophic β-channel to the vertical structure of the equilibrium meridional temperature gradient. *Quart. J. Roy. Meteor. Soc.*, **122**, 55–72, https://doi.org/10.1002/qj.49712252904.
- Santer, B. D., and Coauthors, 2017: Comparing tropospheric warming in climate models and satellite data. *J. Climate*, 30, 373–392, https://doi.org/10.1175/JCLI-D-16-0333.1.
- Screen, J. A., T. J. Bracegirdle, and I. Simmonds, 2018: Polar climate change as manifest in atmospheric circulation. *Curr. Climate Change Rep.*, 4, 383–395, https://doi.org/10.1007/s40641-018-0111-4.
- Seager, R., M. Cane, N. Henderson, D.-E. Lee, R. Abernathey, and H. Zhang, 2019: Strengthening tropical Pacific zonal sea surface temperature gradient consistent with rising greenhouse gases. *Nat. Climate Change*, 9, 517–522, https://doi.org/ 10.1038/s41558-019-0505-x.
- Shaw, T. A., and R. J. Graham, 2020: Hydrological cycle changes explain weak snowball Earth storm track despite increased surface baroclinicity. *Geophys. Res. Lett.*, 47, e2020GL089866, https://doi.org/10.1029/2020GL089866.
- —, and Coauthors, 2016: Storm track processes and the opposing influences of climate change. *Nat. Geosci.*, 9, 656–664, https://doi.org/10.1038/ngeo2783.
- ——, P. Barpanda, and A. Donohoe, 2018: A moist static energy framework for zonal-mean storm-track intensity. *J. Atmos. Sci.*, 75, 1979–1994, https://doi.org/10.1175/JAS-D-17-0183.1.
- Simmons, A. J., and B. J. Hoskins, 1978: The life cycles of some nonlinear baroclinic waves. J. Atmos. Sci., 35, 414–432, https:// doi.org/10.1175/1520-0469(1978)035<0414:TLCOSN>2.0.CO;2.
- Suárez-Gutiérrez, L., C. Li, P. W. Thorne, and J. Marotzke, 2017: Internal variability in simulated and observed tropical

- tropospheric temperature trends. *Geophys. Res. Lett.*, **44**, 5709–5719, https://doi.org/10.1002/2017GL073798.
- Thompson, D. W. J., and T. Birner, 2012: On the linkages between the tropospheric isentropic slope and eddy fluxes of heat during Northern Hemisphere winter. *J. Atmos. Sci.*, **69**, 1811–1823, https://doi.org/10.1175/JAS-D-11-0187.1.
- Thorncroft, C. D., B. J. Hoskins, and M. E. McIntyre, 1993: Two paradigms of baroclinic-wave life-cycle behaviour. *Quart. J. Roy. Meteor. Soc.*, **119**, 17–55, https://doi.org/10.1002/qj.49711950903.
- Trenberth, K. E., and D. P. Stepaniak, 2003: Covariability of components of poleward atmospheric energy transports on seasonal and interannual timescales. *J. Climate*, **16**, 3691–3705, https://doi.org/10.1175/1520-0442(2003)016<3691:COCOPA>2. 0.CO:2.
- Vallis, G. K., P. Zurita-Gotor, C. Cairns, and J. Kidston, 2015: Response of the large-scale structure of the atmosphere to global warming. *Quart. J. Roy. Meteor. Soc.*, **141**, 1479–1501, https://doi.org/10.1002/qj.2456.
- Wheeler, M. C., and H. H. Hendon, 2004: An all-season real-time multivariate MJO index: Development of an index for monitoring and prediction. *Mon. Wea. Rev.*, **132**, 1917–1932, https://doi.org/10.1175/1520-0493(2004)132<1917:Aarmmi>2. 0.Co:2.
- Wilks, D. S., 2011: Statistical Methods in the Atmospheric Sciences. 3rd ed. Elsevier, 676 pp.
- Yoo, C., S. Lee, and S. B. Feldstein, 2012: Arctic response to an MJO-like tropical heating in an idealized GCM. J. Atmos. Sci., 69, 2379–2393, https://doi.org/10.1175/JAS-D-11-0261.1.
- Yuval, J., and Y. Kaspi, 2016: Eddy activity sensitivity to changes in the vertical structure of baroclinicity. J. Atmos. Sci., 73, 1709–1726, https://doi.org/10.1175/JAS-D-15-0128.1.
- —, and —, 2020: Eddy activity response to global warming-like temperature changes. *J. Climate*, **33**, 1381–1404, https://doi.org/10.1175/JCLI-D-19-0190.1.